

**Evidence for robust Bain distortion in the premartensite phase of Ni<sub>2</sub>MnGa magnetic shape memory alloy as a result of 10% Pt substitution**

Sanjay Singh<sup>1</sup>, S. W. D'Souza<sup>1</sup>, M. G. Zavareh<sup>1</sup>, P. Devi<sup>1</sup>, A. S. Gibbs<sup>2</sup>, S. Chadhov<sup>1</sup>,

C. Felser<sup>1</sup> and D. Pandey<sup>3</sup>

<sup>1</sup>Max Planck Institute for Chemical Physics of Solids, Nöthnitzer Strasse 40, D-01187 Dresden, Germany

<sup>2</sup>ISIS Pulsed Neutron Facility, STFC, Rutherford Appleton Laboratory, Chilton, Didcot, Oxfordshire OX11 -0QX, United Kingdom

<sup>3</sup>School of Materials Science and Technology, Indian Institute of Technology (Banaras Hindu University), Varanasi-221005, India.

The premartensite state, considered to be a precursor state of the martensite phase has been intensively investigated in shape memory and magnetic shape memory alloys (MSMAs). The thermodynamic stability of the premartensite phase and its relation to the martensitic phase is still not clear, especially in MSMAs, even though it is critical to understand the functional properties of these alloys. We present here unambiguous evidence for macroscopic symmetry breaking leading to robust Bain distortion of the premartensite phase in Ni<sub>2</sub>MnGa MSMA doped with 10% Pt through a high resolution synchrotron x-ray diffraction study. It is shown that the premartensite phase (T2) with robust Bain distortion results from a “cubic” high temperature premartensite phase (T1) that gets formed first from the cubic austenite phase, through an isostructural phase transition. The martensite phase results from the T2 phase with additional Bain distortion. Our results clearly demonstrate that the premartensite phase should not be considered as a precursor state with the preserved symmetry of the cubic austenite phase. Our work is a major breakthrough in the field of MSMAs as it gives better understanding of the

premartensite state, its relation to the martensite phase transition and the functional properties of these alloys.

The appearance of a precursor state, widely known as premartensite phase, is an interesting feature of compounds/alloys exhibiting martensite phase transitions. This has been extensively studied in conventional shape memory alloys (SMAs), which are a class of materials that remember their shape with respect to change in the temperature and stress<sup>1-9</sup>. These alloys owe the shape memory effect to a phase transition from the high temperature high symmetry austenite phase to a lower symmetry martensite phase. The premartensite state appears in between the parent austenite and martensite phases with preserved parent phase symmetry (cubic) in the sense that the austenite peaks in the diffraction patterns do not exhibit any signature of symmetry breaking or in other words any evidence for Bain distortion. The most characteristic signatures of the premartensite state are the appearance of diffuse streaks and superlattice spots in the x-ray, neutron and electron-diffraction studies<sup>10,11</sup> but the austenite peaks remain unsplit.

Another important class of alloys that owe their functional properties to martensite phase transition are magnetic shape memory alloys (MSMA's), where shape recovery can be realized under the influence of not only the temperature and stress but also the magnetic field. Amongst the MSMAs, stoichiometric Ni<sub>2</sub>MnGa and off-stoichiometric Heusler alloys in the alloy systems Ni-Mn-Ga (In, Sn, Sb) have received considerable attention.<sup>12-21</sup> The stoichiometric Ni<sub>2</sub>MnGa system is by far the most studied system due to its large (10%) magnetic field induced strain (MFIS) with potential for applications in novel multifunctional sensor and actuator devices<sup>13, 14, 22</sup>. It also has potential for applications in magnetic refrigeration through a pronounced magnetocaloric effect<sup>23</sup>. The recent discovery of skyrmions in Ni<sub>2</sub>MnGa has opened newer potential applications for this material in the field of spintronics as well.<sup>24</sup> Ni<sub>2</sub>MnGa is a

multiferroic SMA, as it exhibits two ferroic order parameters, namely spontaneous magnetization and spontaneous strain in the absence of any magnetic field and stress, respectively. The two order parameters appear below the ferromagnetic and ferroelastic (martensite) phase transition temperatures  $T_C \sim 370$  K and  $T_M \sim 210$ K<sup>25, 26</sup>, respectively. The martensitic transition in  $Ni_2MnGa$  is preceded by a premartensite phase transition around  $T=260$  K.<sup>27, 28</sup> Both the martensite and premartensite phases exhibit very strong coupling between the two ferroic order parameters (ie, magneto-elastic coupling) as a result of which  $Ni_2MnGa$  exhibits very large MFIS. The large MFIS is also closely linked with the existence of a long period modulated structure of the martensite phase in the  $Ni_2MnGa$  alloy, as revealed by x-ray, electron and neutron diffraction studies<sup>27, 29-31</sup>. Since the modulated phase of  $Ni_2MnGa$  appears via a modulated premartensite phase and not directly from the austenite phase after its Bain distortion, understanding the characteristics of the premartensite phase and its effect on the martensite phase transformation has been a topic of intense research in recent years<sup>12, 20, 26, 30-39</sup>. The austenite to premartensite transition of  $Ni_2MnGa$  is associated with the softening of the transverse acoustic  $TA_2$  phonon mode at a wave vector  $q \sim 1/3$ <sup>32, 34, 40-42</sup>. Furthermore, temperature dependent photoemission studies on  $Ni_2MnGa$  have revealed the presence of a charge density wave in the premartensite phase<sup>35</sup> with opening of a pseudogap at the Fermi surface indicating Fermi surface nesting leading to appearance of new zone boundaries corresponding to a nearly  $3M(6M$ , see ref<sup>[43]</sup> for this notation) modulated structure of the premartensite state. Both, the austenite-premartensite and the premartensite-martensite transitions are first order in nature, with characteristic thermal hysteresis and phase coexistence regions<sup>28</sup>, due to the strong magnetoelastic coupling between the magnetization and strain caused by the the anomalous  $TA_2$  phonon<sup>12</sup>.

The modulated structure of the premartensite and martensite phases is evidenced by the appearance of weak satellite peaks below the phase transition temperatures  $T_{PM}$  and  $T_M$ , respectively. Recent high resolution synchrotron XRD studies have shown that the nature of the modulation in both the premartensite and martensite phases is incommensurate with nearly  $3M$  and  $7M$  type modulations<sup>26, 28, 44, 45</sup>. It has also been shown using high resolution synchrotron x-ray diffraction that the incommensurately modulated premartensite and the martensite phases coexist over a wide temperature regime across  $T_M$ <sup>28</sup> suggesting that the martensite phase in  $Ni_2MnGa$  originates from the premartensite phase through a first order phase transition. There is, however, a very significant difference between the structures of the premartensite and martensite phases of  $Ni_2MnGa$ . The martensite phase exhibits macroscopic symmetry breaking, as evidenced by pseudotetragonal Bain distortion of the elementary  $L2_1$  cubic unit cell of the austenite phase leading to splitting of the austenite peaks in the diffraction patterns<sup>27, 43</sup>. The premartensite phase, on the contrary, does not exhibit any evidence of symmetry breaking transition as it is always observed with the preserved cubic symmetry of the elementary  $L2_1$  unit cell with no splitting of the basic Bragg peaks of the austenite phase. The only indication of the premartensite transition comes through the appearance of some low intensity satellite peaks below  $T_{PM}$ .<sup>26</sup> In the phenomenological theories of martensite phase transition, the transformation occurs through a lattice deformation shear, with atomic shuffles if necessary, leading to Bain distortion of the austenite unit cell while maintaining an invariant habit plane (contact plane) between the parent and the martensite phases achieved through a lattice invariant shear produced by twinning or stacking faulting<sup>46</sup>. Obviously, it would have been kinetically more favourable if the austenite phase had first undergone a mild Bain distortion in the premartensite phase that could have provided a further path way to the martensite phase transformation with higher Bain distortion while maintaining the integrity of the habit plane all along. In the absence of any macroscopic

Bain distortion, the premartensite phase of  $\text{Ni}_2\text{MnGa}$  does not seem to have a role in facilitating the appearance of Bain distortion in the martensite phase with an invariant habit plane. This then raises a fundamental question as to why at all the premartensite phase arises in  $\text{Ni}_2\text{MnGa}$ . Interestingly, first principles calculations based on purely ground state energies (ie, purely thermodynamic considerations), without considering the kinetic factors required for maintaining an invariant habit plane, predict a global minimum for the “cubic” symmetry of the elementary  $L2_1$  unit cell only. However, these calculations also reveal a local minimum that corresponds to an intermediate value of the Bain distortion in the premartensite phase.<sup>47</sup> The relevant question to be asked then is : “ Can a premartensite phase with an intermediate value of Bain distortion (ie,  $c/a$  ratio) be stabilised to facilitate the development of the martensite phase with full blown Bain distortion with perfect habit plane requirement all through the two transitions?” We seek to answer this fundamental question in this communication.

We present here the first experimental evidence for macroscopic symmetry breaking below  $T_{PM}$  in the premartensite phase of  $\text{Ni}_2\text{MnGa}$  as a result of 10% Pt substitution leading to robust Bain distortion. From high resolution synchrotron XRD data analysis, we show that the Bain distortion grows in steps in the Pt substituted samples. First a nearly 3M modulated premartensite phase with an average “cubic” like feature (ie negligible Bain distortion) of the elementary  $L2_1$  unit cell results from the austenite phase. This phase, however, undergoes an isostructural phase transition to a large Bain distorted 3M like modulated premartensite phase at lower temperatures. Our results establish that the two premartensite phases are stable crystallographic phases and not precursor phases with preserved austenite symmetry, as has been presumed in the literature all along. Further, we also show that the martensite phase originates from the larger Bain distorted premartensite phase suggesting that the Bain distortion appears in steps to facilitate the emergence of an invariant habit plane. These observations, provide us an

opportunity to critically examine the two existing mechanisms of the origin of modulation in these systems.

Polycrystalline sample of  $\text{Ni}_{1.9}\text{Pt}_{0.1}\text{MnGa}$  was prepared by standard arc melting technique. The actual composition of sample was checked by EDX and turns out to be  $\text{Ni}_{1.9}\text{Pt}_{0.08}\text{Mn}_{1.04}\text{Ga}_{0.98}$ . The characteristic (magnetic and structural) transition temperatures were obtained by the ac-susceptibility measurements as a function of temperature using a SQUID-VSM magnetometer. High resolution synchrotron powder x-ray diffraction (SXRPD) measurements were performed at P02 beamline in Petra III, Hamburg, Germany using a wavelength of 0.20712 Å. The time of flight neutron diffraction data were obtained at the ISIS facility (UK) using the high resolution powder diffractometer HRPD at 10 K. For SXRPD and neutron diffraction measurements, the powder samples obtained by crushing the as cast ingots were annealed at 773 K under a high vacuum of  $10^{-5}$  mbar for 10h to remove the residual stresses introduced during grinding<sup>48, 49</sup>. The analysis (Le Bail and Rietveld) of diffraction data were performed using (3+1) D superspace group approach<sup>50-52</sup> with JANA2006 software package.<sup>53</sup>

The *ab-initio* spin polarized DFT calculations have been performed using fully relativistic Korringa–Kohn–Rostoker (SPRKKR) Green function method.<sup>54</sup> The potential has been constructed in the atomic sphere approximation. The electronic exchange and correlation effects are treated by using the generalized gradient approximation (GGA) in the Perdew-Burke-Ernzerhof parametrization scheme.<sup>55</sup> The Brillouin-zone integration was done on a 20X7X14 mesh of k-points. The angular momentum cutoff of  $l_{\text{max}}=2$  (s, p, d orbitals) was used for each atom. The energy convergence criterion was set to  $10^{-5}$  Ry. The structure parameters for  $\text{Ni}_2\text{MnGa}$  were taken from the experiments<sup>26</sup>. For  $\text{Ni}_{1.9}\text{Pt}_{0.1}\text{MnGa}$  we used same structural model as of  $\text{Ni}_2\text{MnGa}$ , except of the volume, which was scaled up to its presently measured experimental value.

The temperature (T) dependence of the ac-susceptibility ( $ac-\chi$ ) of the  $Ni_{1.9}Pt_{0.1}MnGa$  powder sample shown in Fig. 1 reveals a sharp change at paramagnetic-ferromagnetic transition temperature  $T_c \sim 370$  K. On further cooling, the  $ac-\chi$  decreases with a change of slope in the  $\chi$ -T plot around  $T \sim 260$  K. Interestingly, there is another change of slope in  $ac-\chi$  around  $T = 235$  K preceded by a large drop in  $ac-\chi$ . In general, huge drop in  $ac-\chi$  (or dc magnetization in low field) in the Ni-Mn-Ga based MSMA is related with the large magnetocrystalline anisotropy of the martensite phase<sup>56, 57</sup> but Fig. 1 suggests that nearly 40% of the total drop in  $ac-\chi$  in the martensite state has already occurred at 235K in the premartensite phase as a result of 10% Pt substitution. It is important to mention here that Fig. 1 does not exhibit any dip in  $ac-\chi$  for  $Ni_{1.9}Pt_{0.1}MnGa$  at the premartensite phase transition temperature contrary to what is well known in case of stoichiometric  $Ni_2MnGa$ <sup>28</sup>.

Our high resolution SXRPD patterns show clear correlation between the change of slope in the  $\chi$ -T plot and structural changes corresponding to the premartensite and martensite phases discussed above. We show in Fig.2 the variation of SXRPD patterns in selected  $2\theta$  ranges with temperature in the 290-110 K range which captures the entire sequence of phase transitions. The SXRPD pattern at 290K corresponds to the cubic austenite phase as it does not show any splitting of the XRD peaks. The Rietveld refinement using the 290 K data for the cubic structure (Fm-3m space group) shows excellent fit between the observed and calculated peak profiles which further confirms the cubic structure at this temperature (see Fig 3a). The refined cell parameter  $a = 5.84753(6)$  Å obtained from the refinement is slightly higher than that of the stoichiometric  $Ni_2MnGa$  ( $a = 5.82445(1)$  Å), which might be due to the larger atomic size of Pt (1.77 Å) atom compared to the Ni (1.37 Å) atom. This is in good agreement with an earlier study<sup>58</sup> also. On cooling the sample below  $T = 260$  K, several smaller intensity peaks appear. Two such peaks are

marked in the Fig. 2(b) and the inset of Fig 2(b). The low intensity peaks are the satellites that appear due to the modulated nature of the premartensite phase in  $\text{Ni}_2\text{MnGa}$ <sup>28</sup>. The intensity of these satellites increases without much effect on the austenite cubic peaks on further cooling up to  $T=240$  K. The situation is similar to that in  $\text{Ni}_2\text{MnGa}$ , where cooling below the premartensite phase transition temperature ( $T_{\text{PM}}=261$  K) leads to the appearance of low intensity peaks. On the other hand, the austenite peaks remain nearly unaffected and retain their “cubic” nature<sup>28</sup>. The SXRPD of  $\text{Ni}_{1.9}\text{Pt}_{0.1}\text{MnGa}$  in the temperature range 260-240 K thus looks similar to the modulated structure of the premartensite phase of  $\text{Ni}_2\text{MnGa}$ , which is incommensurate with 3M like modulation.<sup>26, 28,27, 29, 31, 59, 60</sup> Therefore we carried out Rietveld analysis of the 240 K SXRPD pattern of  $\text{Ni}_{1.9}\text{Pt}_{0.1}\text{MnGa}$  using the (3+1) D superspace group approach taking into account both the main and the satellite reflections. We use modulated structure of the premartensite phase similar to that of  $\text{Ni}_2\text{MnGa}$  with the superspace group  $Immm(00\gamma)s00$ . The fit between the observed and calculated peak profiles is very good as can be seen from Fig. 3b. The refined lattice parameters at 240 K are found to be:  $a=4.1337(2)$  Å,  $b=5.8416(3)$  Å and  $c=4.1325(1)$  Å with a modulation wave vector ( $\mathbf{q}$ ) of  $\mathbf{q}=0.325\mathbf{c}^*=(1/3-\delta)\mathbf{c}^*$ , where  $\delta=0.0083$  is the degree of incommensuration of modulation at 240 K. The magnitude of  $\mathbf{q}$  confirms the incommensurate nature of modulation. The closest rational approximant to the observed value is  $(1/3)\mathbf{c}^*$  which suggests 3M like modulation in the premartensite phase. Thus the modulated structure of the premartensite phase of  $\text{Ni}_{1.9}\text{Pt}_{0.1}\text{MnGa}$  stable in the temperature range 260-240 K, is identical to the premartensite phase of  $\text{Ni}_2\text{MnGa}$ . The refined lattice parameters and modulation vector are also close to the premartensite phase of  $\text{Ni}_2\text{MnGa}$ <sup>26</sup>.

At  $\sim 235$  K, which is close to the slope change in the  $ac$ - $\chi$  data (marked with the arrow in Fig.1), an interesting feature is observed in the diffraction pattern. It is at this temperature, the splitting

of the Bragg peaks of the cubic austenite structure begins to show (Figs.2d and 2f). However, no additional/new satellite reflections appear. So, this structure corresponds to the premartensite phase only. The satellite peaks are marked with PM in Fig.2b. Later, we will show that this structure is a new premartensite phase having the same 3M like incommensurate modulation but with a robust Bain distortion. This phase is observed up to 225 K while the splitting of cubic austenite peaks continues to increase from 235 K down to 225K. At  $T \sim 220$  K, new peaks have started appearing (marked with M in Figs.2c and 2e and 2f). This is similar to the situation in  $\text{Ni}_2\text{MnGa}$ , where new satellite peaks of martensite phase appear after the premartensite phase is cooled below  $T_M$ <sup>28</sup>. The intensity of these new peaks grows at the expense of the premartensite phase peaks up to 190 K below which the premartensite phase peaks (both main and satellites) disappear completely. Below this temperature (190 K), no additional peaks appear in the structure down to the lowest temperature of our measurement 110K. Thus it can be safely concluded that the martensite structure is stable down to the lowest temperature of measurements (110 K) and even below this temperature as confirmed by our latest neutron scattering measurements.

We investigated the structure of the martensite phase at 110 K by Rietveld refinement in the (3+1) D superspace similar to that in  $\text{Ni}_2\text{MnGa}$ . The main peaks originating from the splitting of the main austenite peaks could be indexed using an orthorhombic unit cell and space group *Immm* as in case of  $\text{Ni}_2\text{MnGa}$ . The unit cell parameters obtained after Le-Bail refinement were found to be  $a = 4.2390$  (1) Å,  $b = 5.5682$  (1) Å and  $c = 4.207412$  (1) Å. The Rietveld refinement was then carried out using the superspace group *Immm* (00 $\gamma$ ) s00 by taking into account the complete diffraction pattern including both the main and satellite reflections. The excellent fit between the observed and calculated profiles (see Fig.3c) confirms that the refinement has

converged successfully. The refined value of the incommensurate modulation vector was found to be  $\mathbf{q} = 0.4290(2) \mathbf{c}^* = (3/7 + \delta) \mathbf{c}^*$ , where  $\delta = 0.00112$  is the degree of incommensuration. Thus the structure at 110 K (which is a representative of the martensite phase stable below 220 K) shows incommensurate modulation similar to the martensite phase of  $\text{Ni}_2\text{MnGa}$ <sup>28, 29, 44, 61</sup>, which is of nearly 7M type.

The structures of the cubic austenite, premartensite phase in the temperature range 260-240 K and the martensite phase at 110 K, which is representative of the structure below 220 K of  $\text{Ni}_{1.9}\text{Pt}_{0.1}\text{MnGa}$  are similar to  $\text{Ni}_2\text{MnGa}$ . However, the structure of the premartensite phase of  $\text{Ni}_{1.9}\text{Pt}_{0.1}\text{MnGa}$  in the temperature range 235-195 K, over which the splitting of the cubic austenite peaks is observed without the presence of the martensite peaks, is quite unusual and we now proceed to analyse this newly observed phase. The splitting of the austenite peaks in the premartensite phase indicates the loss of pseudocubic symmetry of the basic structure. This is completely unexpected for the premartensite phase as it is always considered to be a micromodulated phase with preserved “cubic” symmetry of the austenite peaks. We consider the 225 K data as a representative of this new structure and present the result of fits between calculated and observed intensities by Rietveld refinement. As in the case of the Rietveld refinement of the premartensite and martensite phases stable in the temperature ranges  $245 \text{ K} < T < 260 \text{ K}$  and  $T < 225 \text{ K}$ , respectively we first considered only the main reflections (not satellites) and carried out Le-Bail refinement using the cubic Fm-3m space group. From Fig. 4a, it can be clearly seen that this model misses out the new peaks, which result due to the splitting of the cubic austenite peaks (see the insets of Fig.4a). This confirms that the “cubic” symmetry is now broken. We therefore considered the tetragonal unit cell with space group  $I4/mmm$ , which could capture the splitting but still the observed and calculated peak profiles are not matched

properly. Finally, we took orthorhombic distortion into account in the space group *Immm*, which was used for the martensite phase also. The excellent fit between observed and calculated peak profiles (Fig.4c and inset) shows that at 225 K the basic structure is orthorhombic with refined lattice parameters as :  $a= 4.1356(2) \text{ \AA}$ ,  $b= 5.8276(2) \text{ \AA}$ , and  $c= 4.1371(1) \text{ \AA}$ . There is a clear evidence for the pseudo-tetragonal Bain distortion of the premartensite phase with  $b/\sqrt{2}c \sim 0.9962$ . Having established the Bain distorted orthorhombic nature of the premartensite phase at 225 K, in the next step we carried out Rietveld refinement considering the complete diffraction pattern including satellite reflections using superspace group *Immm*  $(00\gamma) s00$ . An excellent fit between the observed and calculated peak profiles was obtained after the Rietveld refinements (Fig.4d and inset). The refined modulation wave vector  $\mathbf{q}= 0.3393 \mathbf{c}^*$  shows incommensurate nature of the modulation with  $\mathbf{q} = (1/3+\delta) \mathbf{c}^*$ , where  $\delta= 0.0059$  is the degree of incommensuration. Our results using high resolution SXRPD data thus provide evidence for a new incommensurately modulated 3M like premartensite phase with broken cubic austenite symmetry. This is the first example of macroscopic symmetry breaking and Bain distortion in the premartensite phase of any Heusler MSMA.

After establishing the discovery of a new type of the premartensite phase with robust Bain distortion, we now proceed to present evidence for the coexistence of the incommensurate 3M like Bain distorted premartensite and incommensurate 7M like martensite phases below 220 K. For this, we show in Fig.5 the results of Rietveld refinement using the SXRPD pattern at 210 K. It can be observed from the inset of Fig.5a that consideration of only the 3M like incommensurate premartensite phase could not account for some of the Bragg reflections (marked with M in the inset of Fig.5a). We also verified that single phase 7M like incommensurate martensite phase structure cannot account for this diffraction pattern. However,

a refinement based on coexistence of both 3M like Bain distorted premartensite as well as 7M like martensite phases gives an excellent fit between the observed and calculated profiles accounting for all of the peaks (see Fig 5b). From this, we conclude that the Bain distorted 3M like premartensite and 7M like martensite phases, both with incommensurate modulations, coexist at 210 K. Using superspace Rietveld refinement, the coexistence of 3M like and 7M like incommensurate structures was confirmed in the entire temperature range from 210 to 195 K. As phase coexistence is a typical characteristic of a first order phase transition, our result show that the Bain distorted premartensite phase to martensite phase transition is a first order transition. Hence, the martensite phase originates from the premartensite phase in  $\text{Ni}_{1.9}\text{Pt}_{0.1}\text{MnGa}$  also similar to that in  $\text{Ni}_2\text{MnGa}$ .<sup>28</sup> However, there is a major difference in the case of  $\text{Ni}_{1.9}\text{Pt}_{0.1}\text{MnGa}$  since the premartensite phase from which the martensite phase results shows very robust Bain distortion in marked contrast to  $\text{Ni}_2\text{MnGa}$  where the martensite phase results from a premartensite phase that preserves the cubic symmetry of the main unit cell.

Fig.6a shows the variation of the lattice parameters and unit cell volume for the equivalent cubic, premartensite ( $a_{\text{pm}} \approx (1/\sqrt{2}) a_c$ ,  $b_{\text{pm}} \approx a_c$ ,  $c_{\text{pm}} \approx (1/\sqrt{2}) a_c$ ) and martensite ( $a_m \approx (1/\sqrt{2}) a_c$ ,  $b_m \approx a_c$ ,  $c_m \approx (1/\sqrt{2}) a_c$ ) with temperature. It is evident from this figure that unit cell volume for all the phases decreases with decreasing temperature. However, the volume of the cubic austenite phase changes rather smoothly initially during the austenite to premartensite phase transition (260-245 K) similar to that in  $\text{Ni}_2\text{MnGa}$ , as expected for a weakly first order phase transition. However, on lowering the temperature further, a discontinuous change in the volume is observed at  $T \sim 235$  K with a concomitant splitting of the cubic austenite peaks (see Figs.6a & 2f) and change of slope in the  $a_c - \chi$  versus T plot (see Fig.1). This discontinuous change in volume occurs at the ‘‘cubic’’ premartensite to the Bain distorted premartensite phase transition and confirms the first order

nature of this phase transition. Furthermore, a clear discontinuous volume change during Bain distorted premartensite to martensite phase transition is also observed confirming the first order character of this transition as well. The  $b/a$  ratio shown in the inset of Fig.6a also exhibits discontinuous change at temperatures corresponding to the different phases. We believe that the formation of first a cubic premartensite phase in the cubic austenite matrix, followed by a moderately Bain distorted premartensite phase formation in the cubic premartensite matrix and finally the fully Bain distorted martensite phase in the moderately Bain distorted premartensite phase is kinetically more favourable for maintaining an invariant habit plane all through the transition through a sequential evolution of the Bain distortion.

Since, both the premartensite phases belong to the same superspace group  $Immm (00\gamma) s00$  with nearly 3M like incommensurate modulation, this is an isostructural phase transition where the atomic positions shift without changing the Wyckoff site symmetries and the over all space group. The discontinuous change in the unit cell parameters at the isostructural phase transition temperature clearly reveals the presence of strong spin lattice (magnetoelastic) coupling. Isostructural phase transitions are rather rare and have been reported for example in the past during electronic transition in chalcogenides under high pressure<sup>62</sup>, in multiferroics across the magnetic phase transition leading to excess spontaneous polarisation due to magnetoelectric coupling<sup>63-66</sup>, between two ferroelectric phases<sup>67</sup> and between two antiferrodistorted structures in  $\text{CaTiO}_3$ <sup>68</sup>. Our results present the first evidence of an isostructural phase transition between a nearly “cubic” like PM phase and a robust Bain distorted PM phase in a magnetic shape memory alloy.

An incommensurate phase is often perceived to undergo a transition to the “lock- in” commensurate phase at low temperatures in the ground state, as discussed in the literature<sup>69</sup>.

However, our recent high resolution SXRPD study on the stoichiometric Ni<sub>2</sub>MnGa composition reveals that  $q$  vector shows a smooth analytical behavior down to 5 K and there is no evidence for any devilish plateau or commensurate lock-in phase<sup>28</sup>. Since the premartensite in Ni<sub>1.9</sub>Pt<sub>0.1</sub>MnGa shows a robust Bain distortion not present in the stoichiometric composition, it is interesting to investigate the possibility of lock-in phase in this sample. For this, we carried out Rietveld refinement of the structures at various temperatures to determine the modulation wave vector  $\mathbf{q}$  as a function of temperature using Synchrotron XRD data down to 110 K. In addition, we also carried Le Bail refinement using high resolution neutron powder diffraction data at 10 K to verify whether the incommensurate phase would lock-into a commensurate phase in the ground state. The temperature variation of the modulation wave vector  $\mathbf{q}$  is shown in Fig.6b during cooling. A jump in  $q$  is clearly observed at the 3M modulated PM(T1) to PM (T2) isostructural phase transition while both phases continue to remain incommensurate. Furthermore, the incommensurate 3M like PM(T2) to the 7M like incommensurate martensite phase transition is also accompanied with a discontinuous change in the modulation wave vector confirming the first order nature of this transition as well in agreement with the other findings such as discontinuous change in volume and phase coexistence around  $T_M$ . It is interesting to note that the  $q$  for PM (T1) is slightly less than the commensurate value of 0.33 whereas the  $q$  of PM (T2) is slightly greater than 0.33. This implies that the modulation vector remains incommensurate in both the premartensite phases. However, the possibility of  $q$  passing through 0.33 (1/3) commensurate value in the discontinuous jump region with a plateau for  $q=1/3$  cannot be ruled out. From the refinement of the structure using the neutron diffraction data at 10 K(Fig.7), we obtained the lattice parameters as  $a= 4.24452(9)$ ,  $b=5.55035(11)$ ,  $c= 4.20861(8)$  and an incommensurate value of the modulation vector  $q= 0.43238\pm 0.00021$ . This value of  $\mathbf{q}$  confirms that the martensite structure remains incommensurate down to 10 K and shows a smooth

analytical behavior in the entire temperature range of stability of the martensite phase without any intermediate or ground state commensurate lock-in phase in Pt substituted  $\text{Ni}_2\text{MnGa}$  similar to that in the undoped composition.. Thus despite the robust Bain distortion, the ground state seem to remain incommensurate.

We carried out first principles calculations to understand the stability of the Bain distorted premartensite phase assuming a 3M commensurate structure for the stoichiometric  $\text{Ni}_2\text{MnGa}$  with and without 10% Pt substitution. Our calculations clearly reveal not only a global minimum corresponding to the cubic premartensite phase but also a secondary (local) minimum with only a slightly higher energy for a Bain distorted premartensite phase (see Fig.8). We believe that the Bain distorted premartensite phase corresponding to the local minimum becomes stabilised at finite temperatures on account of entropic contributions (Pt disorder), change in the electronic structure due to strong electron phonon interaction as well as strong spin- lattice couplings revealed by discontinuous changes in the unit cell volume at the PM(T1) to PM(T2) and PM(T2) to M phase transitions.

To conclude we have presented the first evidence for robust Bain distortion in the premartensite phase of a MSMA  $\text{Ni}_2\text{MnGa}$  as a result of 10% Pt substitution using high resolution SXRPD. This finding is significant for the field of shape memory alloys in general and MSMA in particular. Our results show that the austenite to martensite phase transition in  $\text{Ni}_{1.9}\text{Pt}_{0.1}\text{MnGa}$  involves three intermediate steps: (i) The first transition is from the austenite to 3M like incommensurate modulated premartensite phase PM (T1), which preserves the “cubic” austenite symmetry of the austenite peaks similar to that in the stoichiometric  $\text{Ni}_2\text{MnGa}$ . (ii) The second transition is an isostructural transition from 3M like incommensurate modulated

premartensite phase (PM(T1)) with negligible Bain distortion to another 3M like incommensurate modulated premartensite phase (PM(T2)) with robust Bain distortion without any change in the superspace group symmetry. (iii) This new 3M like modulated premartensite phase (PM(T2)) finally transforms to the 7M like incommensurate modulated martensite (M) phase. Our results thus suggest that Pt substitution facilitates a gradual increase in Bain distortion which can facilitate the invariant habit plane requirement all through the three transitions until the martensite phase is formed. Our findings have major impact on the physics of origin of modulation in these alloys as it provides a new window of opportunity to critically reevaluate the applicability of the two main theories suggested for the origin of the modulation. The first one is related to the adaptive phase concept, which consider the ground state of the martensite phase to be  $L1_0$  type non-modulated tetragonal structure resulting from the lattice deformation strain (Bain distortion) of the cubic austenite phase. In this model the modulated structure is a metastable phase formed due to kinetic reasons through nanotwinning of the Bain distorted austenite structure. This model does not support the existence of the intermediate premartensite phase and treats the martensite phase as a kinetically stabilized state to overcome the lattice deformation shear causing the Bain distortion<sup>33</sup>. The other theory is based on displacive modulation concept, where the origin of modulation is related to a  $TA_2$  soft acoustic phonon mode of the austenite phase<sup>40</sup>. In the soft mode model an incommensurate modulated martensite phase can result from the incommensurate modulated premartensite phase<sup>28</sup>, both of which are stable thermodynamic phases in their respective range of temperatures. Our results clearly show that the incommensurate martensite phase with larger Bain distortion appears in steps from the Bain distorted premartensite phase. This clearly supports the soft phonon mode based model as the likely origin of modulation in  $Ni_2MnGa$ . This basic understanding of the origin of modulation in

these alloys provides a pathway to design new MSMA's since the large MFIS in Ni<sub>2</sub>MnGa is intimately linked with the existence of the modulated structure.

### **Acknowledgments:**

The work was financially supported by the ERC AG 291472 'IDEA Heusler!' and HeuMem project within the European network M-era.net. Experiments at the ISIS Pulsed Neutron and Muon Source were supported by a beamtime allocation from the Science and Technology Facilities Council. SS thanks Alexander von Humboldt foundation, Germany.

### **References**

- 1 S. M. Shapiro, Y. Noda, Y. Fujii, and Y. Yamada, *Physical Review B* **30**, 4314 (1984).
- 2 S. K. Satija, S. M. Shapiro, M. B. Salamon, and C. M. Wayman, *Physical Review B* **29**, 6031 (1984).
- 3 P. Moine, J. Allain, and B. Renker, *Journal of Physics F: Metal Physics* **14**, 2517 (1984).
- 4 H. Tietze, M. Mullner, and B. Renker, *Journal of Physics C: Solid State Physics* **17**, L529 (1984).
- 5 S. M. Shapiro, B. X. Yang, Y. Noda, L. E. Tanner, and D. Schryvers, *Physical Review B* **44**, 9301 (1991).
- 6 S. M. Shapiro, E. C. Svensson, C. Vettier, and B. Hennion, *Physical Review B* **48**, 13223 (1993).
- 7 L. Ye, S. Shapiro, and H. Chou, *Scripta metallurgica et materialia* **31**, 203 (1994).
- 8 H. Chou and S. M. Shapiro, *Physical Review B* **48**, 16088 (1993).
- 9 T. Ohba, S. Shapiro, S. Aoki, and K. Otsuka, *Japanese journal of applied physics* **33**, L1631 (1994).
- 10 K. Otsuka, T. Sawamura, and K. Shimizu, *Physica status solidi (a)* **5**, 457 (1971).
- 11 G. D. Sandrock, A. J. Perkins, and R. F. Hehemann, *Metallurgical Transactions* **2**, 2769 (1971).
- 12 A. Planes, E. Obradó, A. González-Comas, and L. Mañosa, *Physical Review Letters* **79**, 3926 (1997).
- 13 K. Ullakko, J. K. Huang, C. Kantner, R. C. O'Handley, and V. V. Kokorin, *Applied Physics Letters* **69**, 1966 (1996).
- 14 A. Sozinov, A. A. Likhachev, N. Lanska, and K. Ullakko, *Applied Physics Letters* **80**, 1746 (2002).
- 15 M. Chmielus, X. X. Zhang, C. Witherspoon, D. C. Dunand, and P. Mullner, *Nature Materials* **8**, 863 (2009).
- 16 I. Takeuchi, et al., *Nature Materials* **2**, 180 (2003).
- 17 R. Kainuma, et al., *Nature* **439**, 957 (2006).
- 18 T. Krenke, E. Duman, M. Acet, E. F. Wassermann, X. Moya, L. Manosa, and A. Planes, *Nature Materials* **4**, 450 (2005).
- 19 L. Manosa, D. Gonzalez-Alonso, A. Planes, E. Bonnot, M. Barrio, J.-L. Tamarit, S. Aksoy, and M. Acet, *Nature Materials* **9**, 478 (2010).
- 20 M. A. Uijtewaal, T. Hickel, J. Neugebauer, M. E. Gruner, and P. Entel, *Physical Review Letters* **102**, 035702 (2009).
- 21 Y. Wu, et al., *Scientific Reports* **6**, 26068 (2016).
- 22 S. J. Murray, M. Marioni, S. M. Allen, R. C. O'Handley, and T. A. Lograsso, *Applied Physics Letters* **77**, 886 (2000).
- 23 F.-x. Hu, B.-g. Shen, J.-r. Sun, and G.-h. Wu, *Physical Review B* **64**, 132412 (2001).
- 24 C. Phatak, O. Heinonen, M. De Graef, and A. Petford-Long, *Nano Letters* **16**, 4141 (2016).

25 P. J. Webster, K. R. A. Ziebeck, S. L. Town, and M. S. Peak, *Philosophical Magazine Part B* 49, 295  
(1984).

26 S. Sanjay, J. Nayak, R. Abhishek, R. Parasmani, H. H. Adrian, S. R. Barman, and P. Dhananjai,  
*Journal of Physics: Condensed Matter* 25, 212203 (2013).

27 P. J. Brown, J. Crangle, T. Kanomata, M. Matsumoto, K. U. Neumann, B. Ouladdiaf, and K. R. A.  
Ziebeck, *Journal of Physics: Condensed Matter* 14, 10159 (2002).

28 S. Singh, J. Bednarcik, S. R. Barman, C. Felser, and D. Pandey, *Physical Review B* 92, 054112 (2015).

29 S. O. Mariager, T. Huber, and G. Ingold, *Acta Materialia* 66, 192 (2014).

30 T. Fukuda, H. Kushida, M. Todai, T. Kakeshita, and H. Mori, *Scripta Materialia* 61, 473 (2009).

31 H. Kushida, K. Fukuda, T. Terai, T. Fukuda, T. Kakeshita, T. Ohba, T. Osakabe, K. Kakurai, and K.  
Kato, *Journal of Physics: Conference Series* 165, 012054 (2009).

32 G. Fritsch, V. V. Kokorin, and A. Kempf, *Journal of Physics: Condensed Matter* 6, L107 (1994).

33 S. Kaufmann, U. K. Rößler, O. Heczko, M. Wuttig, J. Buschbeck, L. Schultz, and S. Fähler, *Physical  
Review Letters* 104, 145702 (2010).

34 L. Mañosa, A. Planes, J. Zarestky, T. Lograsso, D. L. Schlagel, and C. Stassis, *Physical Review B* 64,  
024305 (2001).

35 S. W. D'Souza, A. Rai, J. Nayak, M. Maniraj, R. S. Dhaka, S. R. Barman, D. L. Schlagel, T. A.  
Lograsso, and A. Chakrabarti, *Physical Review B* 85, 085123 (2012).

36 B. Benešová, M. Frost, M. Kampschulte, C. Melcher, P. Sedlák, and H. Seiner, *Physical Review B* 92,  
180101 (2015).

37 C. P. Opeil, et al., *Physical Review Letters* 100, 165703 (2008).

38 Y. Wu, et al., *Scientific Reports* 6, 26068 (2016).

39 Y. U. W. a. Y. R. Yongmei M Jin, *npj Computational Materials* 1, 15002 (2015).

40 A. Zheludev, S. M. Shapiro, P. Wochner, and L. E. Tanner, *Physical Review B* 54, 15045 (1996).

41 V. V. Kokorin, V. A. Chernenko, J. Pons, C. Segú, and E. Cesari, *Solid State Communications* 101, 7  
(1997).

42 U. Stuhr, P. Vorderwisch, V. V. Kokorin, and P. A. Lindgård, *Physical Review B* 56, 14360 (1997).

43 S. Singh, S. R. Barman, and D. Pandey, in *Zeitschrift für Kristallographie - Crystalline Materials*,  
2015), Vol. 230, p. 13.

44 S. Singh, V. Petricek, P. Rajput, A. H. Hill, E. Suard, S. R. Barman, and D. Pandey, *Physical Review  
B* 90, 014109 (2014).

45 S. Uba, A. Bonda, L. Uba, L. V. Bekenov, V. N. Antonov, and A. Ernst, *Physical Review B* 94, 054427  
(2016).

46 Z. Nishiyama, *Martensite Transformation* (Academic Press, New York 1978).

47 M. E. Gruner, S. Fähler, and P. Entel, *physica status solidi (b)* 251, 2067 (2014).

48 S. Singh, P. Kushwaha, F. Scheibel, H.-P. Liermann, S. R. Barman, M. Acet, C. Felser, and D.  
Pandey, *Physical Review B* 92, 020105 (2015).

49 S. Singh, M. Maniraj, S. W. D'Souza, R. Ranjan, and S. R. Barman, *Applied Physics Letters* 96,  
081904 (2010).

50 P. De Wolff, *Acta Crystallographica Section A: Crystal Physics, Diffraction, Theoretical and General  
Crystallography* 30, 777 (1974).

51 P. De Wolff, *Acta Crystallographica Section A: Crystal Physics, Diffraction, Theoretical and General  
Crystallography* 33, 493 (1977).

52 T. Janssen, A. Janner, A. Looijenga-Vos, and P. De Wolff, *Mathematical, Physical and Chemical  
Tables* (1992).

53 M. Dušek, V. Petříček, M. Wunschel, R. Dinnebier, and S. v. Smaalen, *Journal of applied  
crystallography* 34, 398 (2001).

54 H. Ebert, D. Ködderitzsch, and J. Minár, *Reports on Progress in Physics* 74, 096501 (2011).

55 J. P. Perdew, K. Burke, and M. Ernzerhof, *Physical Review Letters* 77, 3865 (1996).

56 S. Banik, A. Chakrabarti, U. Kumar, P. K. Mukhopadhyay, A. M. Awasthi, R. Ranjan, J. Schneider,  
B. L. Ahuja, and S. R. Barman, *Physical Review B* 74, 085110 (2006).

57 S. Singh, et al., *Applied Physics Letters* 104, 231909 (2014).

58 S. Singh, S. W. D'Souza, J. Nayak, L. Caron, E. Suard, S. Chadov, and C. Felser, *Physical Review B*  
93, 134102 (2016).

59 H. Kushida, K. Fukuda, T. Terai, T. Fukuda, T. Kakeshita, T. Ohba, T. Osakabe, K. Kakurai, and K.  
Kato, *The European Physical Journal Special Topics* 158, 87 (2008).

- 60 H. Kushida, T. Terai, T. Fukuda, T. Kakeshita, T. Osakabe, and K. Kakurai, *Scripta Materialia* **60**,  
248 (2009).
- 61 L. Righi, F. Albertini, G. Calestani, L. Pareti, A. Paoluzi, C. Ritter, P. A. Algarabel, L. Morellon, and  
M. Ricardo Ibarra, *Journal of Solid State Chemistry* **179**, 3525 (2006).
- 62 A. Jayaraman, *Physical Review Letters* **29**, 1674 (1972).
- 63 S. Lee, et al., *Nature* **451**, 805 (2008).
- 64 A. Singh, V. Pandey, R. K. Kotnala, and D. Pandey, *Physical Review Letters* **101**, 247602 (2008).
- 65 A. Singh, A. Senyshyn, H. Fuess, T. Chatterji, and D. Pandey, *Physical Review B* **83**, 054406 (2011).
- 66 J. P. Patel, A. Senyshyn, H. Fuess, and D. Pandey, *Physical Review B* **88**, 104108 (2013).
- 67 S. Bhattacharjee, K. Taji, C. Moriyoshi, Y. Kuroiwa, and D. Pandey, *Physical Review B* **84**, 104116  
(2011).
- 68 A. K. Saurabh Tripathi, Sharmila Shirodkar, Masatomo Yashima, U. V. Waghmare, Dhananjai  
Pandey, [arXiv:1408.0335](https://arxiv.org/abs/1408.0335) (2014).
- 69 P. Bak, *Reports on Progress in Physics* **45**, 587 (1982).

\

**Figures and captions:**

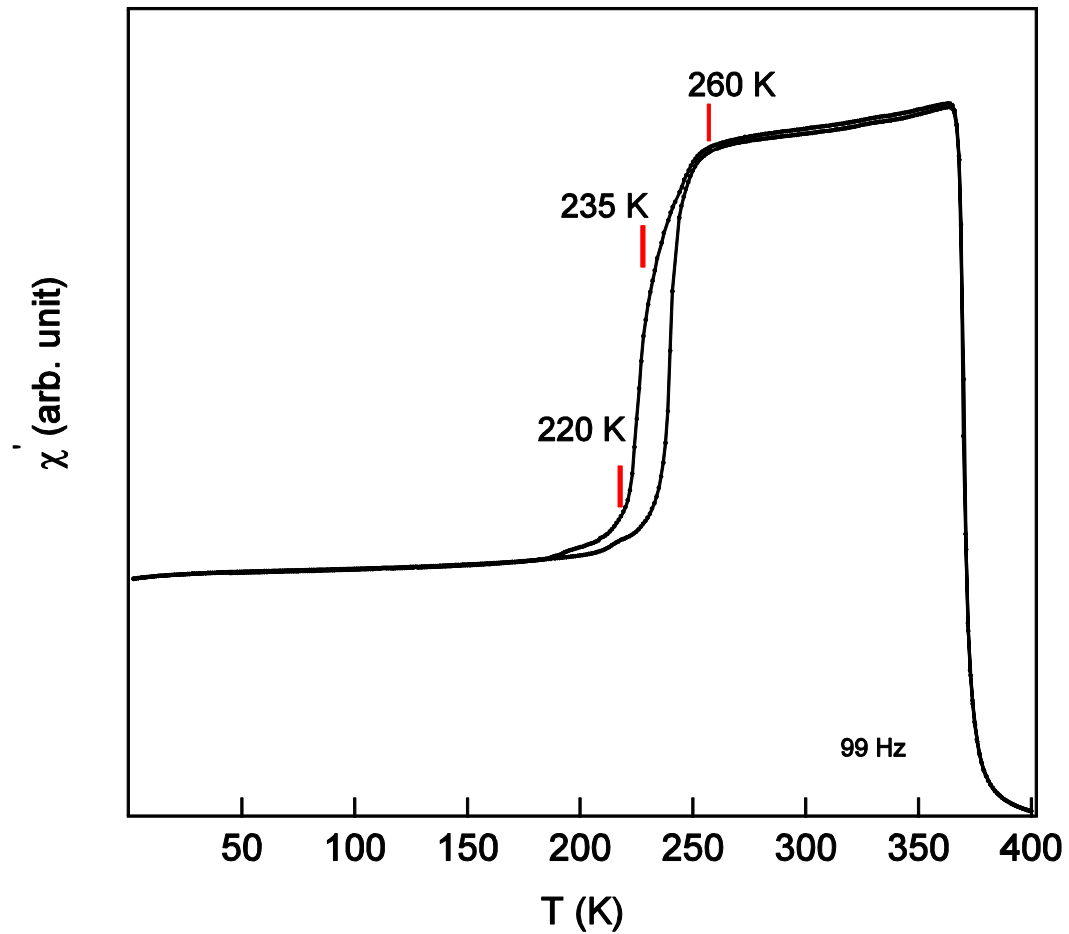


Fig. 1. **Ac-susceptibility:** Real part of ac- $\chi$  as a function of temperature in cooling and heating cycles. Red ticks indicate temperatures correspond to the different phases observed in SXRPD (see text).

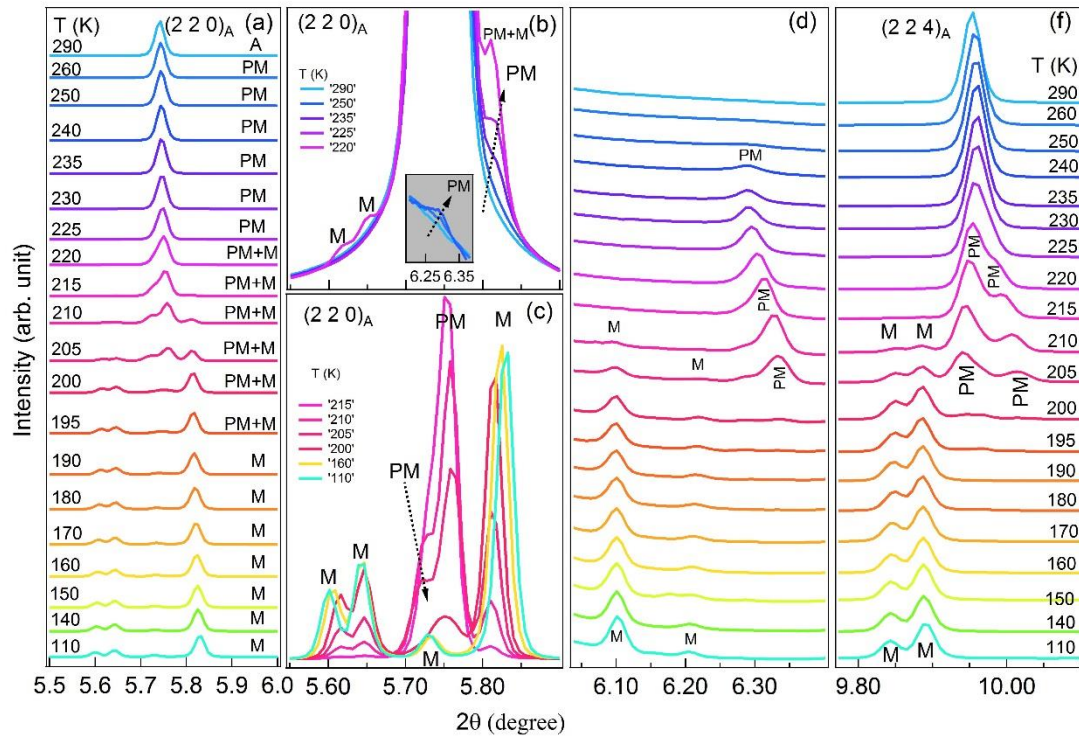


Fig. 2. **Temperature dependent SXRPD patterns:** Evolution of SXRPD patterns of  $\text{Ni}_{1.9}\text{Pt}_{0.1}\text{MnGa}$  as a function of temperature during cooling cycle for 3 selected  $2\theta$  range corresponds to the  $(2\ 2\ 0)_A$  austenite peak region (a), satellite region (d) and  $(2\ 2\ 4)$  austenite peak region (f). (b) and (c) represents  $(2\ 2\ 0)_A$  austenite peak region in an expanded scale for selected temperatures. “A”, “PM” and “M” represent the Bragg peaks due to the cubic austenite, premartensite and martensite phases, respectively. Inset in (b) shows the Bragg reflections on an expanded scale in  $2\theta$  range of 6.20 to 6.38 where satellite reflection of 3M modulated premartensite phase is expected.

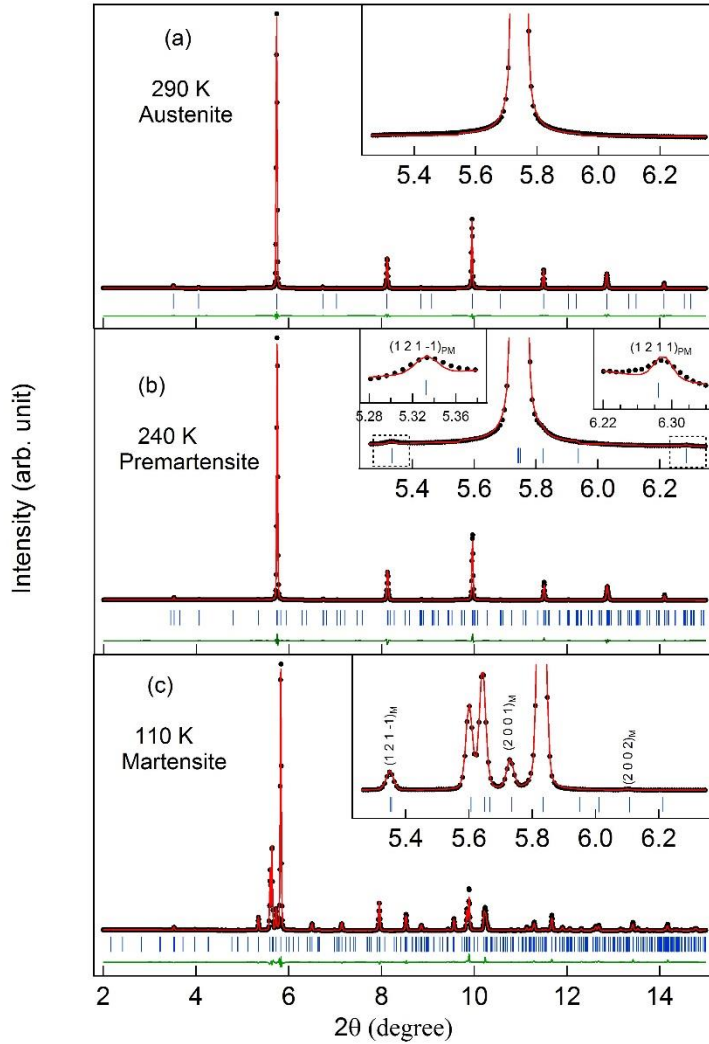


Fig. 3. Rietveld fits for the SXRPD patterns of  $\text{Ni}_{1.9}\text{Pt}_{0.1}\text{MnGa}$ : (a) 290 K (cubic austenite phase), (b) 240 K (premartensite phase) and (c) 110 K (martensite phase). The experimental data, fitted curve and the residue are shown by circles (black), continuous line (red) and bottom most plot (green), respectively. The tick marks (blue) represent the Bragg peak positions. The insets show the fit for the main peak region on an expanded scale. Satellite reflections in the premartensite (PM) and martensite phases (M) are shown by  $(hklm)_{\text{PM}}$  and  $(hklm)_{\text{M}}$ , respectively.

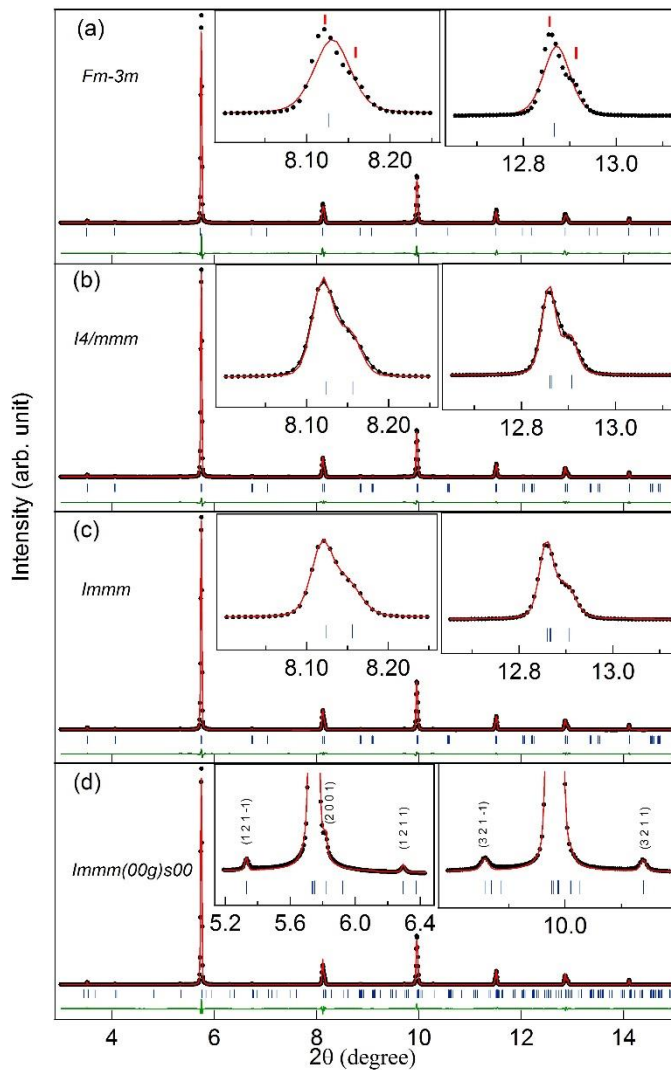


Fig. 4. Rietveld fits for the SXRPD patterns for main peaks at 225 K: (a) with Cubic austenite cell (b) Bain distorted tetragonal unit cell (c) Orthorhombic unit cell. (d) Rietveld fits with 3M modulated incommensurate premartensite structure. The experimental data, fitted curve and the residue are shown by circles (black), continuous line (red) and bottom most plot (green), respectively. The tick marks (blue) represent the Bragg peak positions. The insets in (a), (b) and (c) show the fit for the main reflections and in (d) for satellite reflections corresponding to the premartensite (PM).

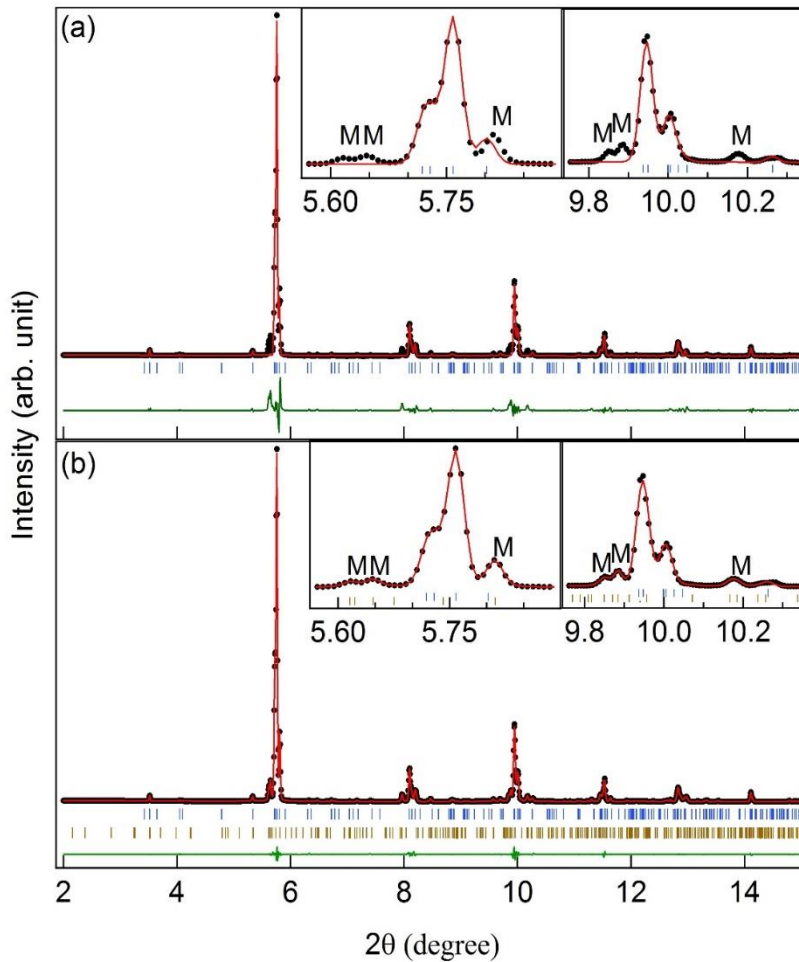


Fig. 5. Rietveld fits for the SXRPD patterns at 210 K: (a) with 3M incommensurate premartensite structure and (b) Combination of 3M premartensite and 7M martensite (M) structure. The experimental data, fitted curve and the residue are shown by circles (black), continuous line (red) and bottom most plot (green), respectively. The tick marks (blue) represent the Bragg peak positions for the premartensite phase and the lower ticks (dark yellow) in (b) represents the Bragg peak positions for the martensite phase. Inset show the Bragg reflections on an expanded scale.

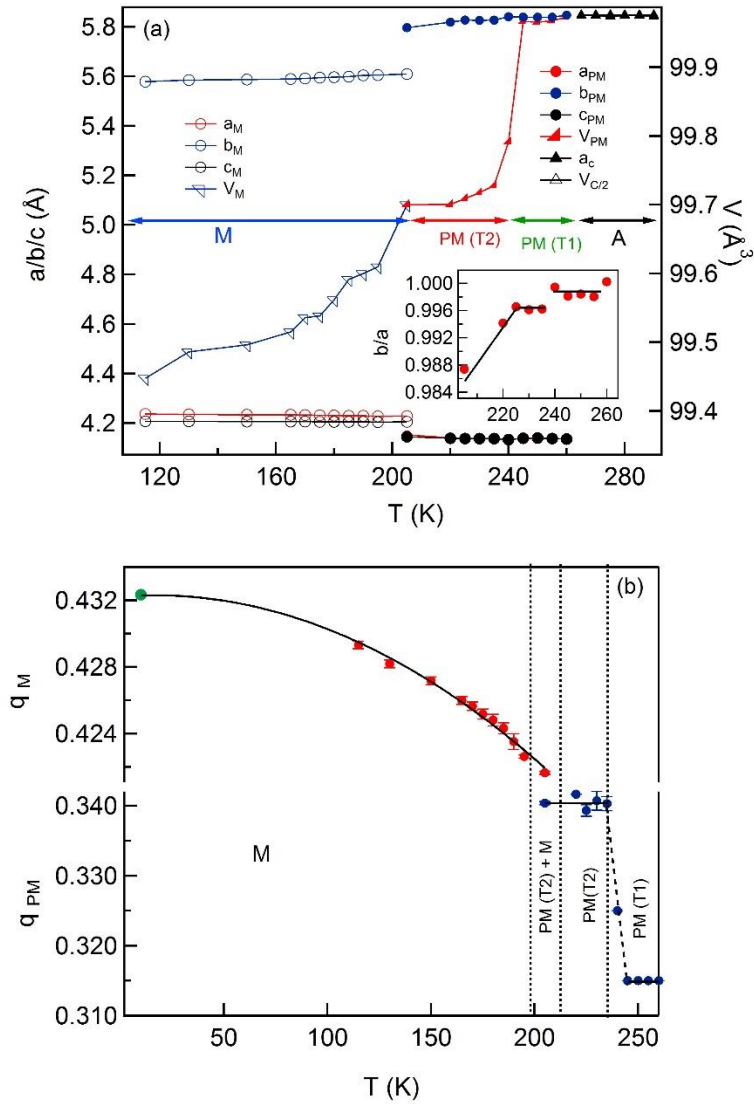


Fig. 6. Temperature variation of the refined parameters: (a) lattice parameters  $a$ ,  $b$ ,  $c$ , and volume in the austenite (A), 3M like premartensite (PM) and the 7M like martensite (M) phase regions for the cooling cycle. The volume of cubic phase is scaled with  $\frac{1}{2}$  for comparison. Inset shows the variation of  $b/a$  ratio (Bain distortion) with temperature in PM (T1) and PM (T2). Subscript c, PM and M are used for austenite cubic, premartensite and martensite phases, respectively. (b) Variation of modulation vector ( $q$ ) as a function of temperature obtained from superspace Rietveld refinements during cooling.

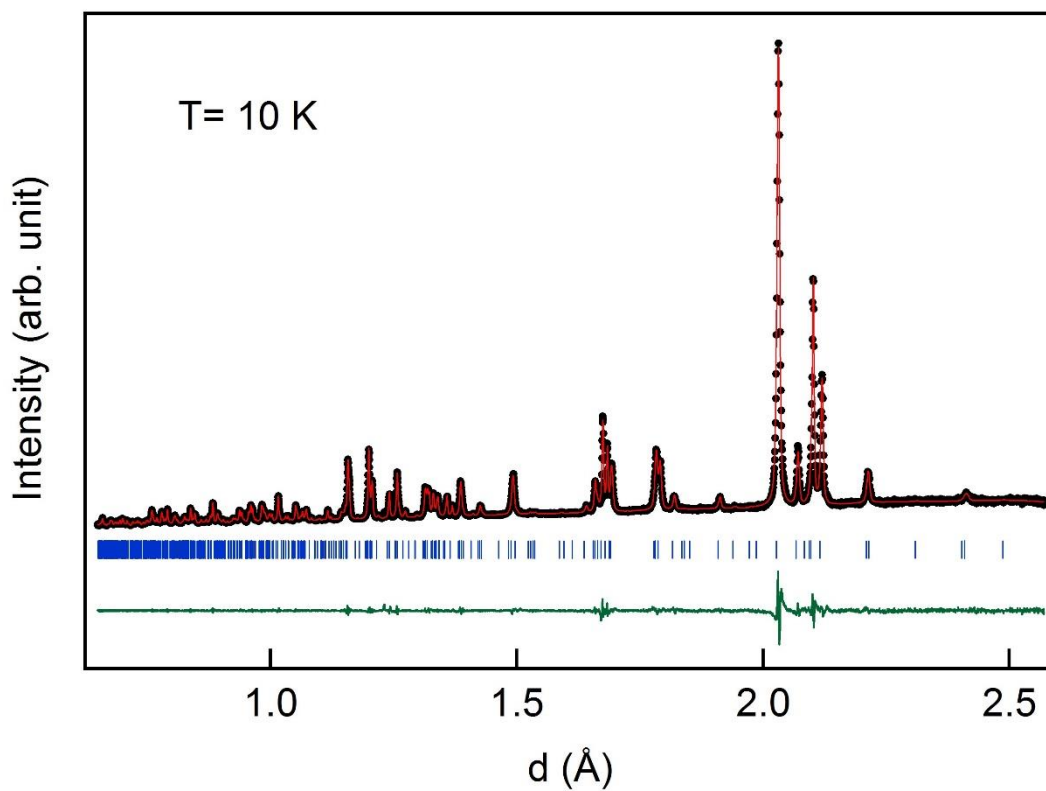


Fig.7. Le Bail fits for the neutron diffraction patterns: The Le bail fitting for high-resolution backscattering bank at 10 K. The experimental data, fitted curve and the residue are shown by circles (black), continuous line (red) and bottom most plot (green), respectively. The tick marks (blue) represent the Bragg peak positions.

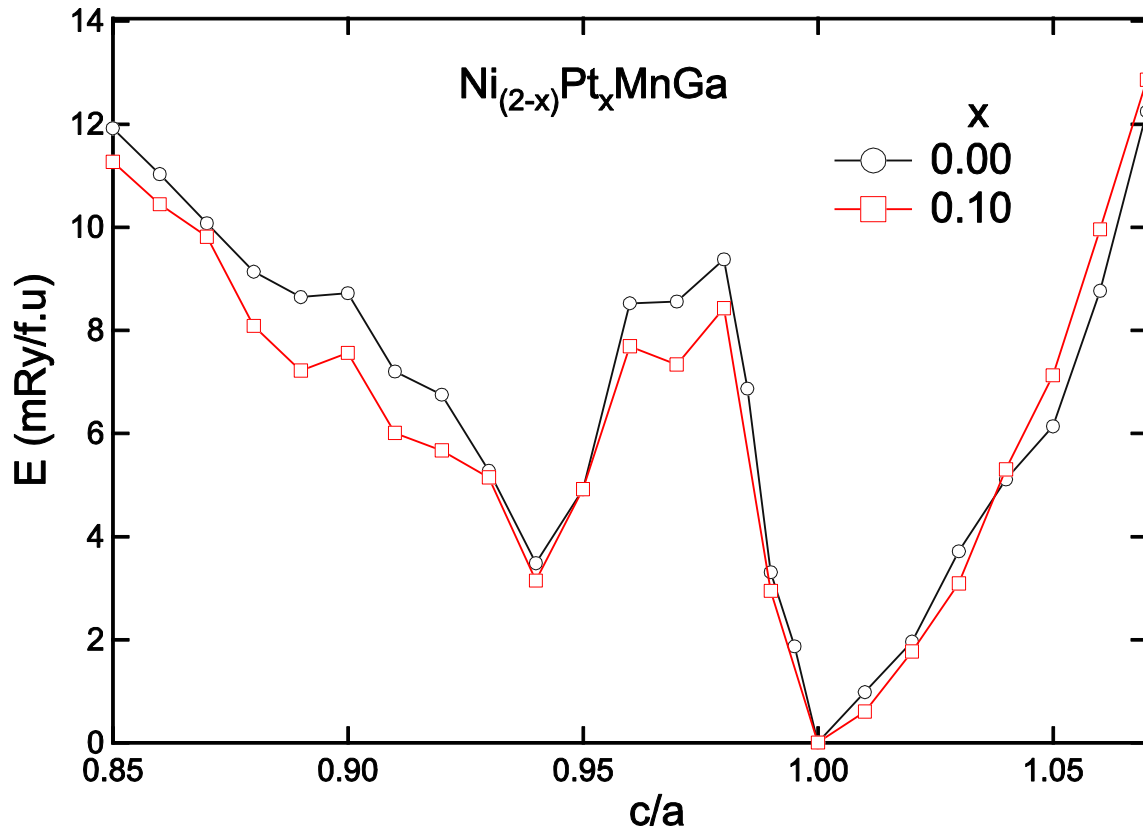


Fig.8: Calculations for energy vs  $c/a$  variation: Theoretical calculation for  $E$  vs  $c/a$  variation of the 3M premartensite phase showing local minimum ( $c/a= 0.94$ ) and global minimum ( $c/a= 1$ ) for  $\text{Ni}_2\text{MnGa}$  and  $\text{Ni}_{1.9}\text{Pt}_{0.1}\text{MnGa}$ .